Journal of Membrane Science 360 (2010) 323–333

Contents lists available at ScienceDirect

Journal of Membrane Science

journal homepage: www.elsevier.com/locate/memsci

# *In silico* screening of zeolite membranes for $CO_2$ capture

Rajamani Krishna*, Jasper M. van Baten

*Van't Hoff Institute for Molecular Sciences, University of Amsterdam, Science Park 904, 1098 XH Amsterdam, The Netherlands*

ARTICLE INFO

*Article history:*
Received 2 April 2010
Received in revised form 3 May 2010
Accepted 8 May 2010
Available online 1 June 2010

*Keywords:*
Zeolites
Monte Carlo simulations
Molecular dynamics
Correlation effects
$CO_2$ capture
Adsorption
Maxwell–Stefan diffusion

ABSTRACT

The separation of $CO_2/H_2$, $CO_2/CH_4$, and $CO_2/N_2$ mixtures is of practical importance for $CO_2$ capture and other applications in the processing industries. Use of membranes with microporous layers of zeolites, metal–organic frameworks (MOFs), and zeolitic imidazolate frameworks (ZIFs) offer considerable promise for use in such separations. In view of the extremely wide variety of available microporous structures, there is a need for a systematic screening of potential candidates in order to obtain the best permeation selectivities, $S_{perm}$. The permeation selectivity is a product of the adsorption selectivity, $S_{ads}$, and the diffusion selectivity, $S_{diff}$, i.e. $S_{perm} = S_{ads} \times S_{diff}$. For maximizing $S_{perm}$, we need to choose materials for which $S_{ads}$ and $S_{diff}$ complement each other.

For a wide variety of zeolites, we have used Configurational-Bias Monte Carlo (CBMC) simulations of mixture adsorption isotherms, along with Molecular Dynamics (MD) simulations of diffusivities for three binary mixtures, $CO_2/H_2$, $CO_2/CH_4$, and $CO_2/N_2$, to calculate $S_{ads}$, $S_{diff}$, and $S_{perm}$. These simulation results provide insights into the influence of pore size, pore topology and pore connectivity that influences each of the three selectivities. In particular, we emphasize the important role of correlations in the diffusion behaviors within microporous materials. Furthermore, we have constructed Robeson plots for each of the separations in order to provide generic guidelines to the choice of materials that offer the appropriate compromise between $S_{perm}$ and the membrane permeability.



## 1. Introduction

Three $CO_2$ separation issues are considered to hold the greatest promise for reducing $CO_2$ emissions [1]. Firstly, we have the problem of separating $CO_2$ and $N_2$ from power plant flue gas streams; this is also termed post-combustion processing. Secondly, in pre-combustion processing of syngas mixtures, $CO_2$ and $H_2$ need to be separated. Thirdly, there is the issue of sweetening of sour natural gas, involving separation of $CO_2$ and $CH_4$. D'Alessandro et al. [1] present a comprehensive survey of the variety of technologies for $CO_2$ capture. On the basis of available information it appears that adsorptive and membrane separations using zeolites, metal–organic frameworks (MOFs), zeolitic imidazolate frameworks (ZIFs), and carbon nanotubes (CNTs) offer energy efficient alternatives to more conventional separation techniques such as amine absorption [1–5].

Fig. 1 illustrates the wide variety of channel topologies and connectivities encountered in zeolites, MOFs, ZIFs, and CNTs. These include: one-dimensional (1D) channels (e.g. AFI, LTL, TON, MTW, CNTs, MIL-47, MIL-53(Cr)), 1D channels with side pockets (e.g. MOR), intersecting channels (e.g. MFI, BEA, ISV, GME, BOG), large cavities with large windows (e.g. FAU, NaX, NaY, IRMOF-1, CuBTC), and cages separated by narrow windows (e.g. LTA, LTA-5A, LTA-4A, CHA, DDR, TSC, ERI, ITQ-29, ZIF-8). The channel or cavity sizes of all of these structures are in the 0.3–2 nm range.

The adsorbent, or microporous membrane layer, with the highest selectivity for a given $CO_2$ separation duty can be selected on the basis of screening of available microporous structures. Palomino et al. [6], for example, have presented an experimental investigation comparing the $CO_2/CH_4$ adsorption selectivity for various cation-exchanged LTA zeolites with ZIFs and MOFs. Experimental screening of potential adsorbents is very time consuming. An alternative approach, as underlined in several recent investigations, is to harness the power of molecular simulation techniques for screening purposes [7–17]. Molecular simulations can be very useful in narrowing down the choices to a handful of promising structures than can be subsequently subjected to more thorough experimental investigations.

Most, if not all, of the screening studies using molecular simulations have focused on the adsorption selectivity, $S_{ads}$, defined by

$$S_{ads} = \frac{c_1/c_2}{f_1/f_2} \quad (1)$$

where the $c_i$ represent the pore concentrations in equilibrium with a bulk fluid phase with partial fugacities $f_i$. We choose to use

* Corresponding author. Tel.: +31 20 6270990; fax: +31 20 5255604.
*E-mail address:* r.krishna@uva.nl (R. Krishna).

0376-7388/$ – see front matter © 2010 Elsevier B.V. All rights reserved.
doi:10.1016/j.memsci.2010.05.032

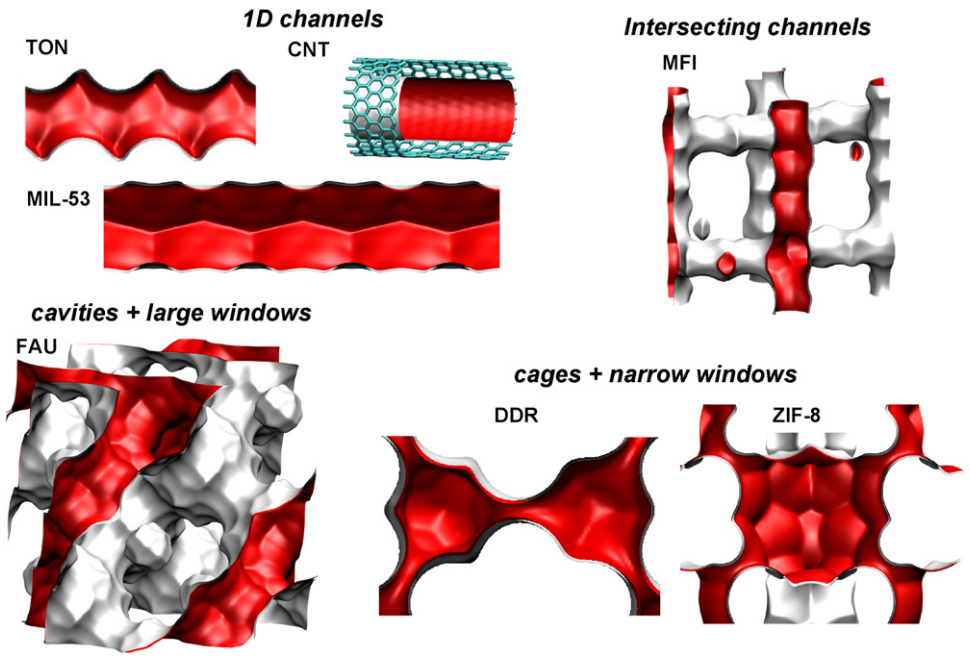


**Fig. 1.** Examples of the variety of channel topologies and connectivities in zeolites, MOFs, ZIFs, and CNT. Details of the specific structures are available in the Supplementary Material accompanying this article.

fugacities, $f_i$, in Eq. (1) instead of partial pressures, $p_i$, because in many cases of $CO_2$ capture the pressures encountered are high, in the 1–6 MPa range, and thermodynamic non-idealities are non-negligible. Furthermore, in molecular simulations performed in the grand canonical ensemble, the $f_i$ are directly accessible.

For membrane processes, the main focus of the present communication, it is of relevance to examine the permeation selectivity, $S_{perm}$, defined by

$$S_{perm} = \frac{N_1/N_2}{f_1/f_2} \tag{2}$$

where the $N_i$ are the permeation fluxes across the membrane for partial gas phase fugacities $f_i$ in the upstream membrane compartment. For microporous membranes, the permeation fluxes are most conveniently described using the Maxwell–Stefan (M–S) equations [17–20]

$$-\phi\frac{c_i}{RT}\nabla\mu_i = \sum_{\substack{j=1\\ j\neq i}}^{2}\frac{c_jN_i - c_iN_j}{c_t Đ_{ij}} + \frac{N_i}{Đ_i}, \quad i = 1, 2 \tag{3}$$

where $\phi$ represents the fractional pore volume of the microporous crystalline material, and the concentrations $c_i$ are defined in terms of accessible pore volume of the crystalline microporous layer.

The $Đ_1$ and $Đ_2$ are the M–S diffusivities of the pure components 1 and 2; these represent the interactions between the component species and the pore walls. For any guest species, the $Đ_i$ values vary by several orders of magnitude depending on the pore size and topology; they are also dependent on the loading or concentration within the pores as is illustrated for diffusivity of $CO_2$ in a variety of microporous structures; see Fig. 2a. The channel size is an important determinant for the magnitude of the diffusivity; for the chosen structures, the highest selectivity is for MIL-53(Cr) that has 8.5 Å sized channels, while the lowest diffusivity is for DDR that has cages separated by windows that are $3.6 \times 4.4$ Å in size. Consider the three structures FAU, NaY (54 $Na^+$), and NaX (86 $Na^+$) that have the same pore topology with pore size of 7.4 Å, but with increasing number of cations. Increasing the number of cations increases the adsorption strength of $CO_2$, due to increased electrostatic interactions. This is witnessed by the pure component isotherms in Fig. 2b. The $Đ_i$ values for $CO_2$ have the inverse hierarchy FAU > NaY > NaX; this is because the "sticking tendency" increases with adsorption strength leading to lower diffusivities [17]. A higher sticking tendency, implies a lower mobility.

The $Đ_{12}$ are exchange coefficients that capture correlation effects in molecular jumps from one adsorbed site to another. The ratios $Đ_1/Đ_{12}$ and $Đ_2/Đ_{12}$ quantify the degree of correlations [17,19,20]. For any guest mixture, the ratios $Đ_1/Đ_2$, $Đ_1/Đ_{12}$, and $Đ_2/Đ_{12}$ vary over several orders of magnitude depending on the pore size, topology, and connectivity of the host structure. To illustrate this, Fig. 2c compares the values of $Đ_1/Đ_{12}$ for $CO_2(1)/H_2(2)$ mixture diffusion in variety of structures. One-dimensional structures such as MTW, and TON have the highest degree of correlations. This is followed by the intersecting channel structure of MFI, and the large pore FAU structure. The lowest degree of correlations are encountered in LTA, CHA, DDR, and ERI that have cages separated by narrow 0.32–0.45 nm sized windows. Another point to note is that the degree of correlations generally increases as the concentration inside the pores increases. A qualitative appreciation of the differences in the diffusion characteristics between the various structures can also be appreciated by viewing video animations of MD simulation diffusion that has been provided as Supplementary Material. Video animations 1–3 illustrate the "single file" nature of diffusion in 1D channels of TON and MIL-47, leading to strong correlations in molecular jumps. Video 4 illustrates the jumps of $CO_2$ and $CH_4$ in the intersecting channels of MFI; here the intersections act as "traffic junctions" serving to increase the degree of correlations between jumps $CO_2$ and $CH_4$. Videos 5 and 6 give a feel for diffusion of $CO_2$ and $CH_4$ within the "open" structures of NaY and NaX, also showing interactions with mobile cations. Videos 7–12 given an appreciation of the hopping of guest molecules across the narrow windows of LTA, CHA, DDR, and ZIF-8. We note that only one molecule at a time can pass a window, causing the diffusion process to be practically uncorrelated.

The permeation selectivity can be expressed as

$$S_{perm} = S_{ads} \times S_{diff} \tag{4}$$

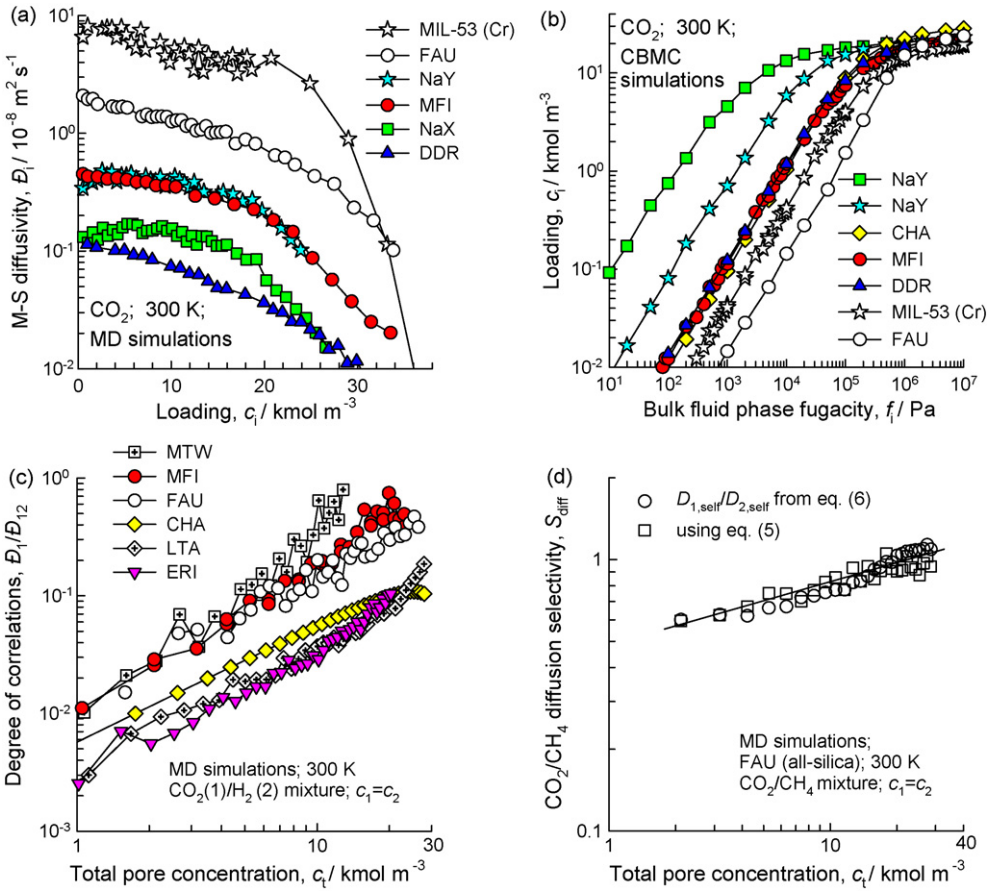


**Fig. 2.** (a) M–S diffusivity $Đ_i$, from MD simulations for pure $CO_2$ in a variety of microporous materials a function of $c_i$. (b) CBMC simulation data for isotherms of $CO_2$ in a variety of microporous materials. (c) The degree of correlations, $Đ_1/Đ_{12}$, for $CO_2(1)/H_2(2)$ mixture diffusion a variety of zeolites. (d) Comparison of the estimations of $S_{diff}$ using Eqs. (5) and (6) for $CO_2/CH_4$ mixture diffusion in all-silica FAU.

where $S_{diff}$ is the diffusion selectivity. Starting with Eq. (3), the following expression for $S_{diff}$ can be derived

$$S_{diff} = \frac{Đ_1}{Đ_2}\frac{1+(Đ_2/Đ_{12})}{1+(Đ_1/Đ_{12})} \tag{5}$$

As a very good approximation, the right member of Eq. (5) can be taken equal to the ratio of the self-diffusivities $D_{i,self}$ in the mixture

$$S_{diff} = \frac{D_{1,self}}{D_{2,self}} \tag{6}$$

The detailed derivations of Eqs. (5) and (6) are provided in the Supplementary Material accompanying this publication; see also earlier published work [21,22]. The use of Eq. (6) is particularly convenient because the $D_{i,self}$ are more easily accessible by use of Molecular Dynamics (MD) simulations than the $Đ_1$, $Đ_2$ and $Đ_{12}$.

As illustration, Fig. 2d compares the estimations of $S_{diff}$ using Eqs. (5) and (6) for $CO_2/CH_4$ diffusion in all-silica FAU. The agreement between the two sets of results is extremely good.

From the point of view of selecting optimum microporous structures, it is useful to identify two limiting scenarios for the correlations. When correlations are negligibly small, $(Đ_1/Đ_{12}) \to 0$; $(Đ_2/Đ_{12}) \to 0$ either Eq. (5) or (6) degenerates to yield

$$S_{diff} = \frac{Đ_1}{Đ_2};\ \text{correlations negligible} \tag{7}$$

This scenario implies that $S_{diff}$ can be estimated on the basis of experimental pure component permeance data. Eq. (7) holds as a good approximation for structures such as CHA, DDR, LTA, TSC, ERI, and ZIF-8 that have cages separated by narrow windows. The molecules hop one-at-a-time across the windows, and the hopping rates are practically uncorrelated.

The other extreme scenario is one in which correlation effects are dominant, i.e. $(Đ_1/Đ_{12}) \gg 0$; $(Đ_2/Đ_{12}) \gg 0$ yielding

$$S_{diff} = 1;\ \text{correlations dominant} \tag{8}$$

When Eq. (8) holds, $S_{perm} = S_{ads}$. Eq. (8) holds as a good approximation for 1D channel structures such as CNTs [19].

The main objective of the present communication is to highlight the possibilities of enhancing the permeation selectivities by proper choice of the microporous structure that offers the best diffusion selectivities. We shall underline the importance of choosing the structure that has the right degree of correlations for a specified separation application. We shall demonstrate that, for any given separation, we aim to satisfy either Eq. (7) or (8). For illustrating a variety of concepts we consider the separation of three different binary mixtures $CO_2/H_2$, $CO_2/CH_4$, and $CO_2/N_2$ that are relevant for $CO_2$ capture. Additionally, a few simulations were also carried out with $CH_4/H_2$ and $CH_4/N_2$ mixtures in order to underline the generic applicability of the presented concepts. In all cases, we determined $S_{ads}$ by use of Configurational-Bias Monte Carlo (CBMC) simulations of mixture adsorption. Additionally, $S_{diff}$ was determined from MD simulations of the $D_{i,self}$. The entire data base of simulation results is available in the Supplementary Material accompanying this publication; this material includes details of the CBMC and MD simulation methodologies, details of the microporous structures investigated (unit cell dimensions, accessible pore volume, characteristic pore dimensions), pore landscapes, specification of the force fields used, simulation data on mixture isotherms, $S_{ads}$, and $S_{diff}$.

Most of the investigated structures are zeolites, chosen carefully to reflect the different classes of pore topologies and connectivities portrayed in Fig. 1. For comparison purposes we also investigated a few typical MOFs (CuBTC, IRMOF-1, MIL-53), ZIFs (ZIF-68, ZIF-8), and CNTs.

In performing molecular simulations, we assume perfect, defect-free, crystals, and rigid crystalline frameworks. These assumptions are considered to be reasonable for purposes of screening, the focus of the current study. However, for more accurate design purposes, it may be necessary to take other factors into consideration, such as surface resistance or inter-crystalline resistance of crystals [23,24], and framework flexibility influences [25–27]. Framework flexibility issues are of particular importance when the guest molecules are tightly constrained as for example in inter-cage hopping across the narrow windows of CHA, DDR, LTA, and ZIF-8 [28]. In MOFs such as MIL-53, guest-induced structural transformations may occur, and this needs special analysis [29,30].

We begin our discussions by considering the adsorption selectivities.

## 2. Adsorption selectivities

$CO_2$ has a larger quadrupole moment ($14.3 \times 10^{-40}$ C m$^2$), and a higher polarizability ($26.3 \times 10^{-25}$ cm$^3$) than any of the partner molecules $H_2$, $CH_4$, and $N_2$. Consequently, $CO_2$ has the higher adsorption strength in all three mixtures. As illustration, Fig. 3 shows the CBMC simulations of the component loadings in NaX zeolite for $CO_2(1)/N_2(2)$ mixtures in equilibrium with a bulk fluid phase, with partial fugacities $f_1/f_2 = 15/85$. For a fair comparison of the loadings in various structures, it is necessary to express the loadings, $c_i$, in terms of moles per m$^3$ of accessible pore volume [17,20,31]. In this context, it is worth pointing out that many microporous structures contain pockets or cages that are not accessible in experiments. In CBMC simulations, it is important to block such regions in order to obtain a fair representation of experimental reality [32]. For example, the sodalite cages in LTA, ITQ-29, FAU, TSC need to be blocked as these are inaccessible to guest molecules. Also, DDR zeolite contains pockets that need blocking [32,33]. The molecular simulation screening study of Liu and Smit [11] must be treated with caution because the inaccessible pockets of LTA and DDR were not blocked [32]. For every structure, the accessible pore volume was determined with the aid of molecular simulations using the helium probe insertion technique suggested by Talu and Myers [34,35]. The details of the technique used and the pore volume data are provided in the Supplementary Material, which also contains data such as that shown in Fig. 3 for all guest mixtures in all the chosen host materials.

From the CBMC simulated component loadings, the adsorption selectivities, $S_{ads}$, can be calculated by use of Eq. (1). Let us first consider $S_{ads}$ for $CO_2/H_2$ mixtures; this problem is encountered in pre-combustion applications. Fig. 4a summarizes the adsorption

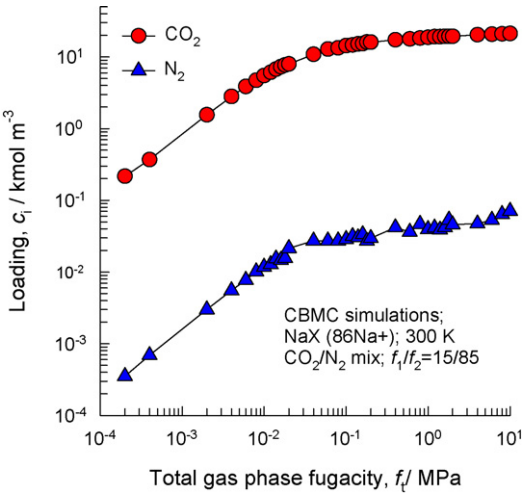


**Fig. 3.** CBMC simulations for the component loadings $c_i$ in equilibrium with binary fluid phase mixtures $CO_2(1)/N_2(2)$ in NaX (106 Si, 86 Al, 86 Na$^+$, Si/Al = 1.23) at 300 K. The partial fugacities in the bulk fluid phase are such that $f_1/f_2 = 15/85$. The complete set of CBMC data for all mixtures in all microporous hosts available in the Supplementary Material accompanying this publication.

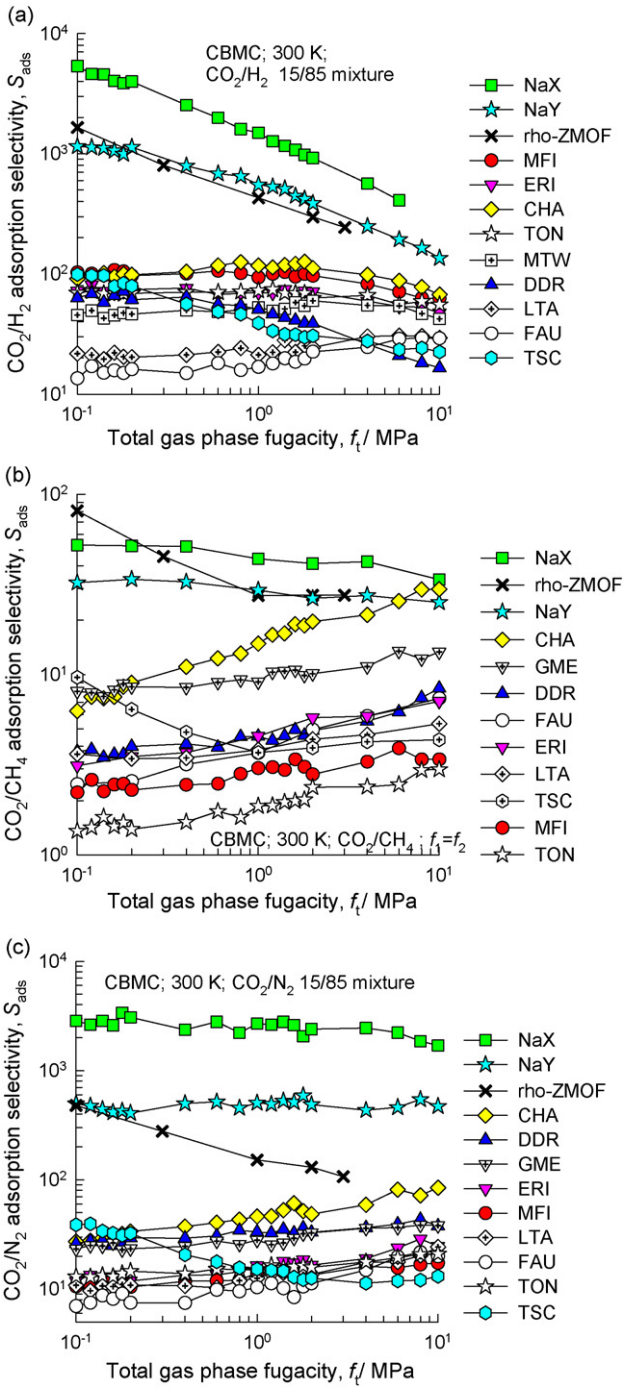


**Fig. 4.** Adsorption selecivities, $S_{ads}$, for (a) $CO_2(1)/H_2(2)$, (b) $CO_2(1)/CH_4(2)$, and (c) $CO_2(1)/N_2(2)$ mixtures in a variety of microporous materials, plotted as a function of the total bulk fluid phase fugacity, $f_t = f_1 + f_2$. For clarity of presentation, only a selection of the simulation data are presented here; the complete set of data are available in the Supplementary Material accompanying this publication.

selectivities, $S_{ads}$, for $CO_2(1)/H_2(2)$ mixtures as a function of the total gas phase fugacity, $f_t = f_1 + f_2$. In all structures $S_{ads} \gg 1$. The highest $S_{ads}$ is obtained with NaX (86 $Na^+$). Comparing the $S_{ads}$ values for the same FAU topology we find the following hierarchy NaX (86 $Na^+$) ≫ NaY (54 $Na^+$) ≫ FAU (all-silica). A similar hierarchy holds for $CO_2(1)/CH_4(2)$ and $CO_2(1)/N_2(2)$ mixtures; see Fig. 4b and c. These data underline the strong increase in $S_{ads}$ with increasing number of cations present. This increase is to be attributed to enhanced electrostatic interactions of the cations with $CO_2$. The significant role of electrostatic interactions for $CO_2$ adsorption has been underlined in the literature [11,16]. The adsorption selectivities are also enhanced by incorporation of special functional groups within a framework. For example, the work of Couck et al. [36] demonstrates that functionalizing the MIL-53(Al) metal–organic framework with amino groups increases its selectivity in $CO_2/CH_4$ separations by orders of magnitude while maintaining a very high capacity for $CO_2$ capture. An and Rosi [37] demonstrate the possibility of enhancing the $CO_2$ adsorption selectivity in MOFs by introduction of cations.

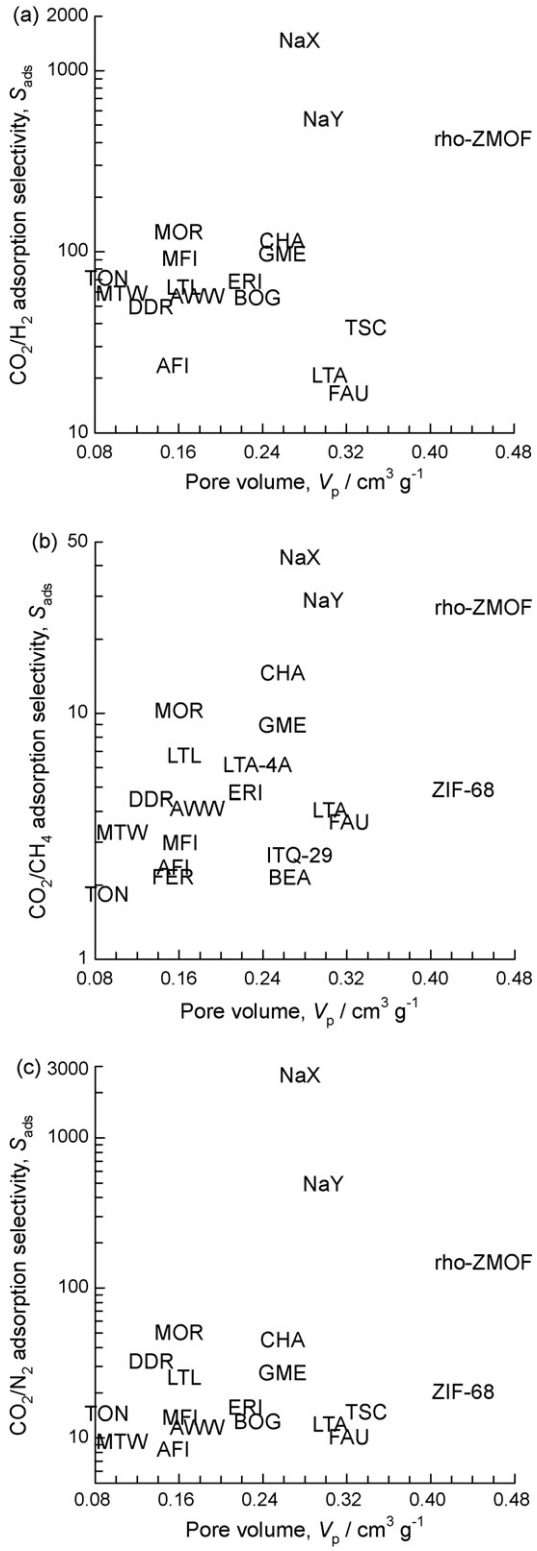


**Fig. 5.** Adsorption selecivities, $S_{ads}$, for (a) $CO_2(1)/H_2(2)$, (b) $CO_2(1)/CH_4(2)$, and (c) $CO_2(1)/N_2(2)$ at a total bulk fluid phase fugacity $f_t = 1$ MPa, plotted as a function of the pore volume of the microporous material.

In a recent simulation study of RHO-zeolite-like metal–organic framework, Babarao and Jiang [38] found extremely high selectivities, significantly higher than 50, for $CO_2/H_2$, $CO_2/CH_4$, and $CO_2/N_2$ adsorption due to electrostatic interactions of $CO_2$ with the charges of the anionic framework atoms and charge-balancing extra-framework $Na^+$ ions. Their selectivity values for rho-ZMOF are also plotted in Fig. 4a–c. It is interesting to note that for total gas phase fugacities, $f_t$, exceeding 0.2 MPa, NaX and NaY exhibit values of $S_{ads}$ that are higher than that for rho-ZMOF. The statement of Babarao and Jiang [38] in their paper "The predicted selectivities in rho-ZMOF are the highest reported to date among various MOFs and unprecedentedly higher than those for other porous materials" needs to be revised in light of the data presented in this work.

Fig. 5 presents a comparison of $S_{ads}$ for the three mixtures at total bulk fluid phase fugacity $f_t = 1$ MPa, typical of several $CO_2$ capture technologies, using the pore volume $V_p$ of the various microporous materials on the $x$-axis. Such a comparison is useful from a practical point of view, because $V_p$ is a reflection of the capacity of material for adsorption. The upper right corner of these plots are the desirable regions, with both high selectivities and high capacities for adsorbing guest molecules. NaX, NaY, and rho-ZMOF are three structures that emerge as the best ones using this criterion. It is of particular practical interest to note that the best adsorption selectivities are obtained with a widely used commercial adsorbent such as NaX.

## 3. Diffusion and permeation selectivities

The diffusion selectivity $S_{diff}$ is dictated by a variety of factors that include molecular dimensions, pore size, connectivity, and adsorption strength. Fig. 6 presents cartoons showing approximate molecular dimensions of the gases investigated in this work;

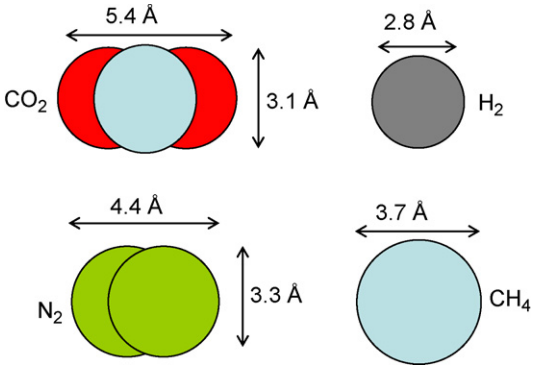


**Fig. 6.** Cartoon showing the approximate molecular dimensions of $CO_2$, $H_2$, $N_2$, and $CH_4$. The molecular diameters are estimated on the basis of the Lennard–Jones size parameters $\sigma$ for molecule–molecule interactions. The molecular lengths are estimated on the basis of the bond lengths.

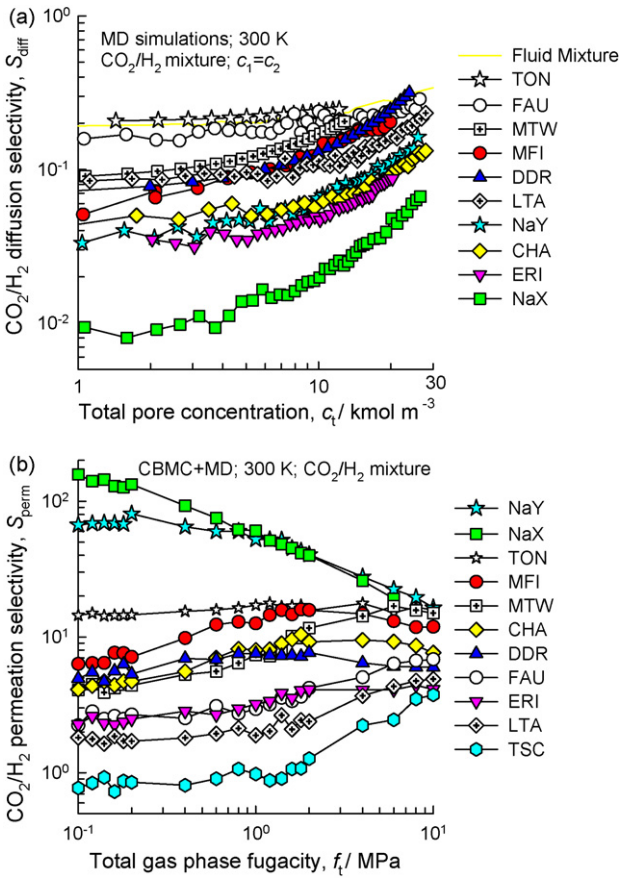


**Fig. 7.** (a) Comparison of diffusion selectivities, $S_{diff}$, for equimolar ($c_1 = c_2$) $CO_2/H_2$ mixtures at 300 K, plotted as a function of the total pore concentration $c_t = c_1 + c_2$. (b) Permeation selectivities, $S_{perm}$, for $CO_2/H_2$ mixtures, plotted against the total bulk gas phase fugacity, $f_t$.

these dimensions were estimated using published force fields for molecule–molecule interactions [39–43]. The cartoons will be helpful in appreciating the trends in the $S_{diff}$ that invariably do not go hand-in-hand with $S_{ads}$.

### 3.1. $CO_2/H_2$ mixtures

Due to the much smaller molecular size of $H_2$ molecules, the $S_{diff}$ in all microporous structures is lower than unity, as witnessed by MD simulation results for equimolar (i.e. $c_1 = c_2$) $CO_2(1)/H_4(2)$ mixtures in Fig. 7a. For the same FAU topology we find the $S_{diff}$ values for FAU, NaY, and NaX to be 0.24, 0.055, and 0.018 for a pore concentration of 10 kmol $m^{-3}$, a hierarchy that is opposite to that for $S_{ads}$. Increasing adsorption strength by enhancing the electrostatic interactions of $CO_2$ with $Na^+$ has the effect of reducing the mobility of $CO_2$ due to increased "sticking" tendency [17]. This is true in most cases, and for membrane permeation this essentially means that $S_{diff}$ counteracts the gain in $S_{ads}$. Also shown in Fig. 7a are the $S_{diff}$ values for a fluid mixture at the same molar concentration as within the pores. The value of $S_{diff}$ for a fluid mixture is an "upper bound" and provides a target of $CO_2$-selective operations. If we aim for a membrane separation process that is selective to $CO_2$, we should choose micropore topologies that yield $S_{diff}$ values as close to the fluid mixture value as possible. This is achievable by choosing structures in which the degree of correlations are very strong, and for which the differences in the mobilities of $CO_2$ and $H_2$ get washed out. One-dimensional channel structures such as CNT, TON and MTW allow this possibility. Indeed we find that for TON, $S_{diff}$ is very close to that of the fluid mixture. Video 1 gives a visual appreciation of the high degree of correlations in TON; the more mobile $H_2$ cannot bypass the tardier $CO_2$, and "single file" diffusion prevails.

We can combine the information presented in Figs. 4a and 7a to obtain the $S_{perm}$, using Eq. (4). For this purpose, the $S_{diff}$ values are determined at the total fluid concentration $c_t = c_1 + c_2$, with the component loadings $c_i$ from data such as shown in Fig. 3. The $S_{perm}$, plotted in Fig. 7b, reflect a balance between the $S_{ads}$ and $S_{diff}$. For an upstream membrane fugacity $f_t = 1$ MPa, typical for pre-combustion separations [1], the zeolites with the highest $S_{perm}$ are obtained with NaY, NaX, TON, MTW, and MFI.

From a membrane process development viewpoint, a more appropriate approach is not to select membranes based just on $S_{perm}$, but to also consider the $CO_2$ permeability of the membrane, $\Pi_i$, defined by

$$\Pi_i = \frac{N_i}{\Delta f_i / \ell} \tag{9}$$

where $\ell$ is the thickness of the crystalline layer on the membrane. If the downstream conditions are such that the loadings are negligibly small, the $CO_2$ permeability can be determined from MD simulations by using the following expression

$$\Pi_i = \frac{\phi D_{i,self} c_i}{f_i} \tag{10}$$

where $c_i$ is the pore concentration of $CO_2$ at the upstream face of the membrane. Detailed derivations of Eq. (10) are provided in the Supplementary Material. For a chosen upstream total fugacity $f_t = 1$ MPa, the conventionally used Robeson plot [44] can be constructed in which the permeation selectivities are plotted against the $CO_2$ permeability, $\Pi_i$, expressed in Barrers; see Fig. 8. NaY offers the best combination of $S_{perm}$ and $\Pi_i$. The good performance of NaY can be attributed to three different reasons: (1) high $S_{ads}$ due to electrostatic interactions of $CO_2$ with cations, (2) high permeability due to the large and "open" pore structure, and (3) high degree of correlations in such open structures. For the same set of reasons, we should also expect a material such as amine functionalized MIL-53 to offer comparable performance in terms of $S_{perm}$ and $\Pi_i$. The 1D channels of MIL-53 offer a high degree of correlations that are desirable [17]. For use of 1D channel structures in membrane permeation devices, there is however a practical issue relating to the orientation, and alignment of all 1D channels.

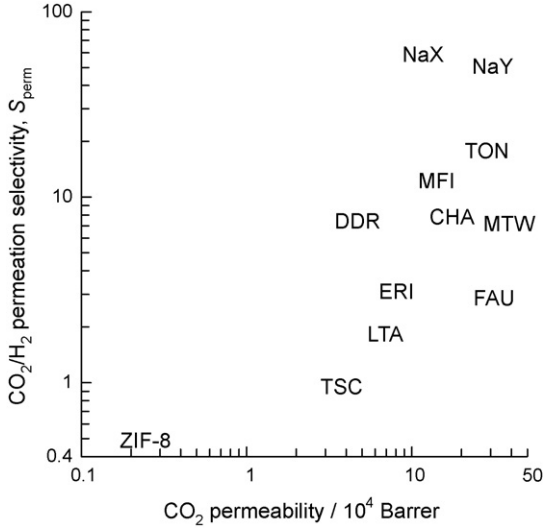


**Fig. 8.** Robeson plot for separation of $CO_2/H_2$ mixtures, with total upstream fugacity $f_t = 1$ MPa, and $T = 300$ K. The permeation selectivities, $S_{perm}$, for different microporous structures are plotted against the $CO_2$ permeability, $\Pi_i$. Note that the $x$-axis is expressed in $10^4$ Barrers.

A different approach is to aim for a $H_2$-selective membrane separation. This is possible if we allow $S_{diff}$ to overpower $S_{ads}$ by choosing microporous structures that act as $H_2$-sieves. One candidate structure is ZIF-8 that is a structural analog of SOD zeolite. The windows separating the cages are about 0.34 nm in size [45,46], allowing $H_2$ to diffuse through much more easily than $CO_2$; see snapshot in Fig. 9a. For this strategy to be more effective, it is advantageous to operate at higher temperatures, where the adsorption selectivity in favor of $CO_2$ is reduced; see Fig. 9b. At a temperature of 500 K, the comparison of $S_{ads}$, $S_{diff}$, and $S_{perm}$, is shown in Fig. 9c. We note that $H_2/CO_2$ permeation selectivities of the order of 50 are anticipated by a combination of CBMC and MD simulations. There is recent experimental evidence in the literature to confirm that such a $H_2$-selective separation is possible with ZIF-7, that has a structure similar to that of ZIF-8 [47]. Video 11 illustrates the rapid inter-cage hopping of $H_2$ across the windows of ZIF-8, while $CO_2$ can be seen to be predominantly engaged in intra-cage hops.

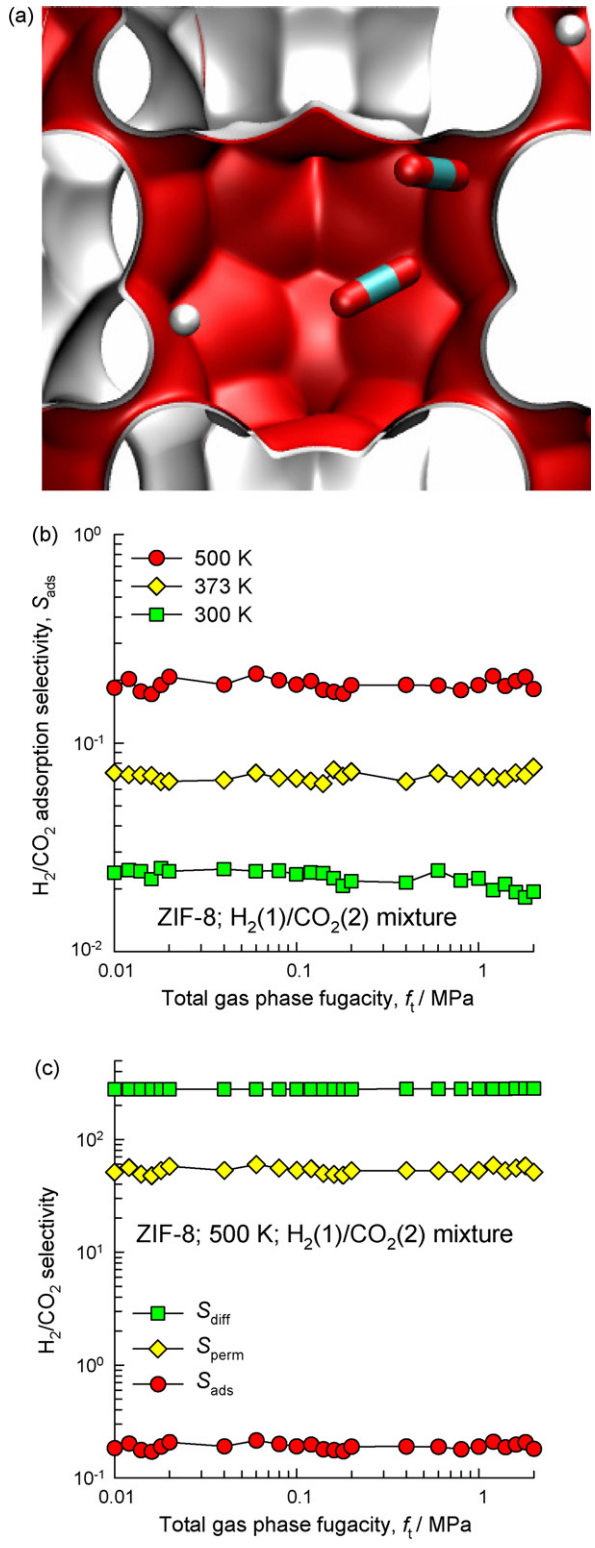


**Fig. 9.** (a) Snapshot showing the location of $CO_2$ and $H_2$ within a ZIF-8 cage. (b) Comparison of $S_{ads}$ for separation of $CO_2/H_2$ mixture at 300 K, 373 K, and 500 K in ZIF-8. (c) Comparison of $S_{ads}$, $S_{diff}$, and $S_{perm}$, for separation of $CO_2/H_2$ mixture at 500 K in ZIF-8.

### 3.2. $CH_4/H_2$ mixtures

The foregoing concepts and considerations for $CO_2/H_2$ mixtures also apply to $CH_4/H_2$ separations, relevant for $H_2$ recovery from fuel gas or natural gas streams. For $CH_4$-selective separation, we should aim for 1D structures with a high degree of diffusional correlations. Carbon nanotubes are excellent choices in this regard, and this is evidenced by molecular simulation results for $CH_4/H_2$ permeation selectivities that are summarized in Fig. 10a. The earlier studies of Chen and Sholl [48] also confirm the efficacy of CNTs for this task. Structures such as ZIF-8, LTA, and CHA, that have narrow windows separating cages, allow $H_2$-selective permeation and there is

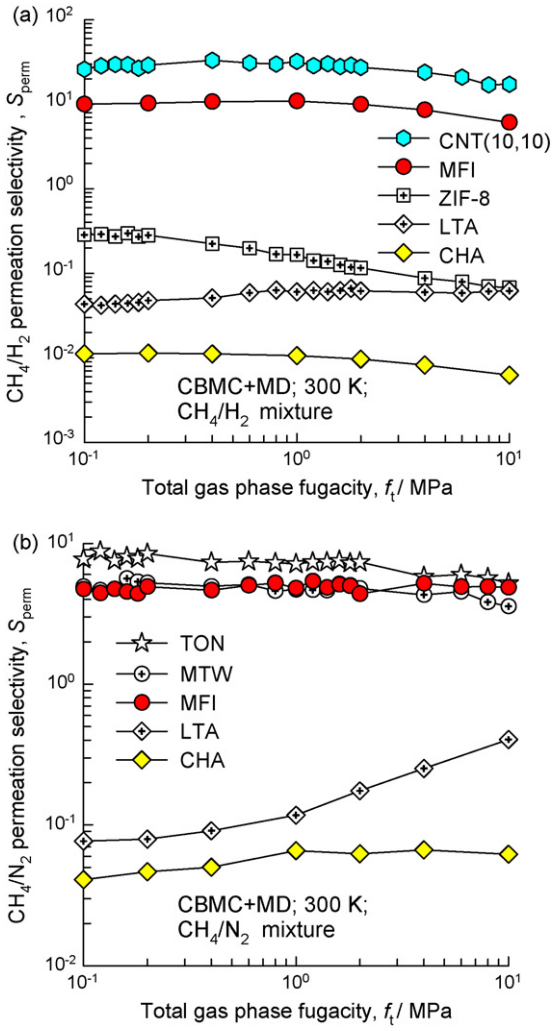


**Fig. 10.** Comparison of $S_{perm}$ for separation of (a) $CH_4/H_2$, and (b) $CH_4/N_2$ mixtures at 300 K in a variety of microporous structures.

experimental evidence of such separations in the published literature [45,46,49]. Video 12 illustrates the rapid inter-cage hopping of $H_2$ across the windows of ZIF-8, while $CH_4$ can be seen to be predominantly engaged in intra-cage hops.

### 3.3. $CH_4/N_2$ mixtures

Nitrogen is a common contaminant in natural gas, and requires removal because it reduces the calorific value of the fuel and makes it unsaleable. For $CH_4/N_2$ separations, the permeation selectivity is in favor of $CH_4$ in microporous structures such as TON, MTW, and MFI in which diffusional correlation effects are significantly high; see Fig. 10b. Conversely, for structures such as LTA and CHA, for which correlation effects are negligibly small, the permeation selectivities are in favor of $N_2$. Experimental data [49] for $CH_4/N_2$ permeation across a SAPO-34 membrane, an iso-type of CHA, confirm the predictions of Fig. 10b.

### 3.4. $CO_2/N_2$ mixtures

The molecular sizes of $CO_2$ and $N_2$ are comparable (cf. Fig. 6), and consequently the diffusion selectivities in a given material are higher than for $CO_2/H_2$ mixtures. The hierarchy of $S_{diff}$ is however the same as for $CO_2/H_2$ mixtures. The $S_{perm}$ values, along with the Robeson plot, are summarized in Fig. 11a and b. Our $S_{perm}$ estimate for MFI of 8.2 is in reasonable agreement with the experiments of Bernal et al. [50]. The best combination of $S_{perm}$ and $\Pi_i$. values are obtained with NaX and NaY zeolites, a conclusion that is essentially the same as for $CO_2$-selective $CO_2/H_2$ separation. There is evidence that the predicted permeation selectivities for NaY can indeed be realized in experiments [51–54]. This is useful from practical view point because for $CO_2$-selective separation of pre- and post-combustion processes the same material (i.e. NaY) works the best, and therefore process development can be focused on just one material. However, $N_2$-selective separation of $CO_2/N_2$ does not appear to be feasible.

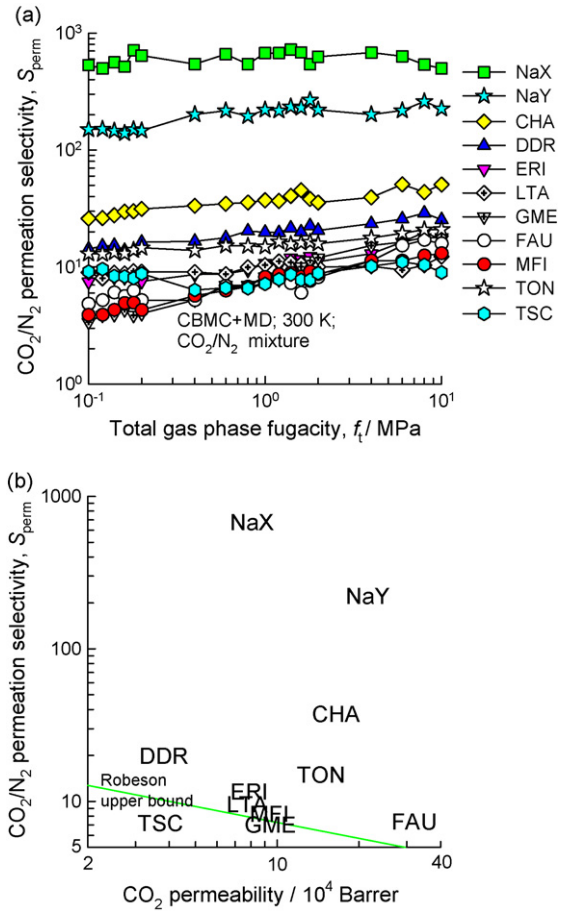


**Fig. 11.** (a) Permeation selectivities, $S_{perm}$, for $CO_2/N_2$ mixtures, plotted against the total bulk gas phase fugacity, $f_t$. (b) Robeson plot for separation of $CO_2/N_2$ mixtures, with total upstream fugacity $f_t = 1$ MPa, and $T = 300$ K. The permeation selectivities, $S_{perm}$, for different microporous structures are plotted against the $CO_2$ permeability, $\Pi_i$. Note that the $x$-axis is expressed in $10^4$ Barrers. Also plotted is the "upper bound" calculated using the parameters specified in Table 12 of Robeson [44].

### 3.5. $CO_2/CH_4$ mixtures

Let us now analyze the diffusional selectivities for $CO_2/CH_4$ mixtures. In 1D channels, intersecting channels, and open structures for which the pore sizes are larger than about 0.55 nm, the diffusion selectivities $S_{diff} < 1$; see Fig. 12a. This is mainly due to the fact that the higher adsorption strength of $CO_2$, lowers its mobility within the micropores.

$CO_2$ is a more slender molecule than $CH_4$ (cf. Fig. 6) and a different scenario holds for ERI, CHA, ITQ-29, DDR, TSC, and LTA. For these structures, the $S_{diff}$ is significantly higher than unity; see Fig. 12b. This is because the linear $CO_2$ molecule hops length-wise across the narrow 0.35–0.45 nm sized windows. This is best evidenced by viewing the animations in Videos 7–11 for LTA, DDR, and CHA zeolite. Furthermore, the preferential location of $CO_2$ at the window regions of LTA, and DDR serves to hinder the inter-cage hopping of $CH_4$; this explains why $S_{diff} \gg 1$ [55,56]. The hierarchy of $S_{diff}$ in Fig. 12b is dictated, broadly speaking, by the hierarchy of window

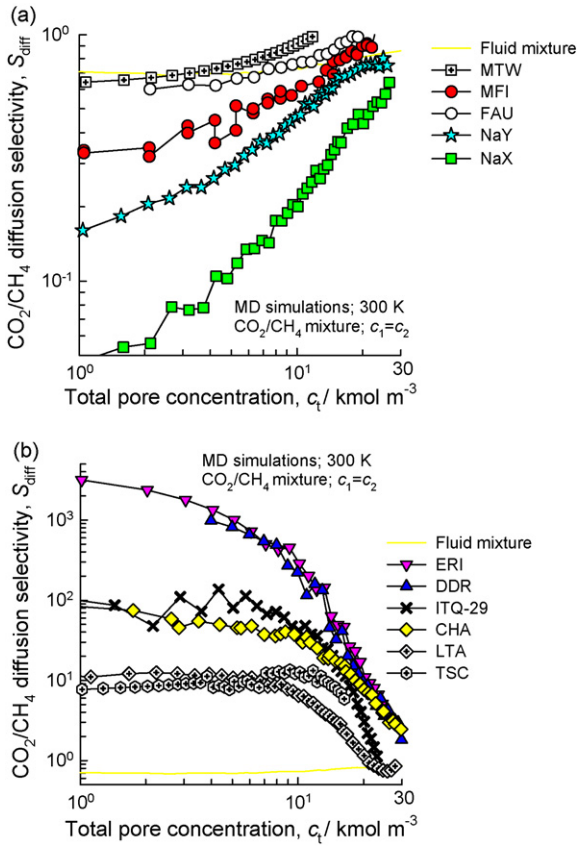


**Fig. 12.** (a and b) Comparison of diffusion selectivities, $S_{diff}$, for equimolar ($c_1 = c_2$) $CO_2/CH_4$ mixtures at 300 K plotted as a function of the total pore concentration $c_t = c_1 + c_2$. For clarity of presentation only a selection of the simulation data are presented here; the complete set of data are available in the Supplementary Material accompanying this publication.

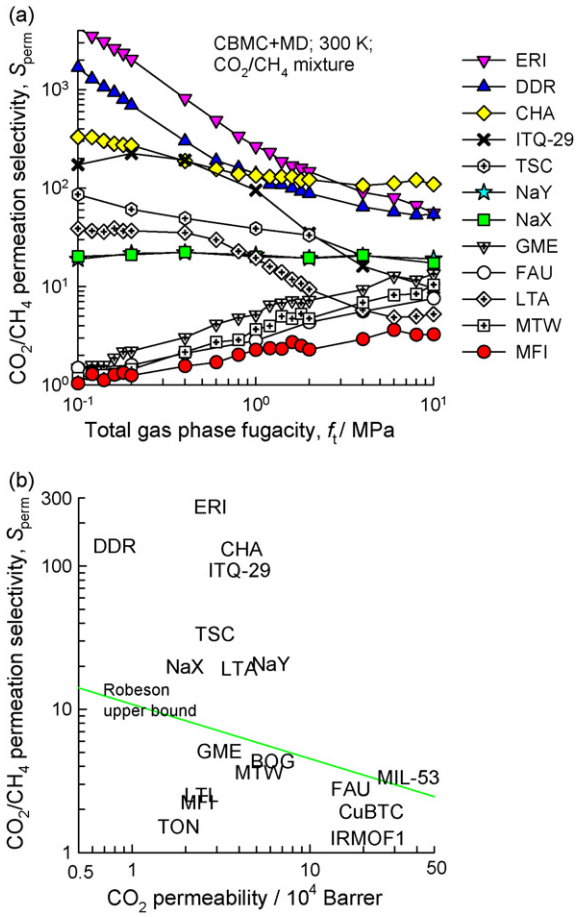


**Fig. 13.** (a) Permeation selectivities, $S_{perm}$, for $CO_2/CH_4$ mixtures, plotted against the total bulk gas phase fugacity, $f_t$. (b) Robeson plot for separation of $CO_2/CH_4$ mixtures, with total upstream fugacity $f_t = 1$ MPa, and $T = 300$ K. The permeation selectivities, $S_{perm}$, for different microporous structures are plotted against the $CO_2$ permeability, $\Pi_i$. Note that the $x$-axis is expressed in $10^4$ Barrers. Also plotted is the "upper bound" calculated using the parameters specified in Table 12 of Robeson [44].

sizes; the smaller the window size, the higher is the value of $S_{diff}$. Unlike for the four foregoing mixtures discussed above, there is a possibility of enhancing $S_{perm}$ by choosing topologies such as ERI, CHA, ITQ-29, DDR, TSC, and LTA in which correlation effects are negligible.

The permeation selectivities $S_{perm}$, plotted in Fig. 13a, reflect the combined influences of adsorption and diffusion. For an upstream membrane fugacity $f_t = 1$ MPa, typical of natural gas sweetening applications, the $S_{perm} > 100$ are obtained with ERI, DDR, and CHA. For DDR and CHA, there is experimental evidence that such high permeation selectivities can be realized in practice [49,56–61]. For MFI, the $S_{perm}$ value of 2.3 is in agreement with experiment [60]. Fig. 13b presents the Robeson plot for $CO_2/CH_4$ mixture separation in all the microporous structures that we have investigated. Open, large pore, structures such as FAU, MIL-53, IRMOF-1, and CuBTC have high $\Pi_i$ but low $S_{perm}$. On the other hand, ERI, DDR, and CHA have significantly higher $S_{perm}$ values but with lower $\Pi_i$. For technological applications, a compromise has to be struck. The compromise structure could perhaps be NaY with a relatively high permeability, or CHA, with a high $S_{perm}$. There is considerable scope for development of novel materials that would lead to a performance at the top right corner. The strategy should be to aim to develop frameworks such as MIL-53, with 1D channels in which strong functional groups are attached to ensure strong $CO_2$ adsorption.

It is also interesting to note that for both $CO_2/N_2$ and $CO_2/CH_4$ separations, the separation performance of a few zeolites exceeds the upper bound of Robeson [44]; see Figs. 11b and 13b.

### 3.6. Comparison with experimental data

It remains to provide experimental proof that the predictions of the permeation selectivity trends using molecular simulations are a fair reflection of actual experimental data. Fig. 14a presents a collection of the experimental data of Li et al. [49,60] on permeation selectivities, $S_{perm}$, for $CO_2/CH_4$, $CO_2/N_2$, $CO_2/H_2$, $CH_4/N_2$,

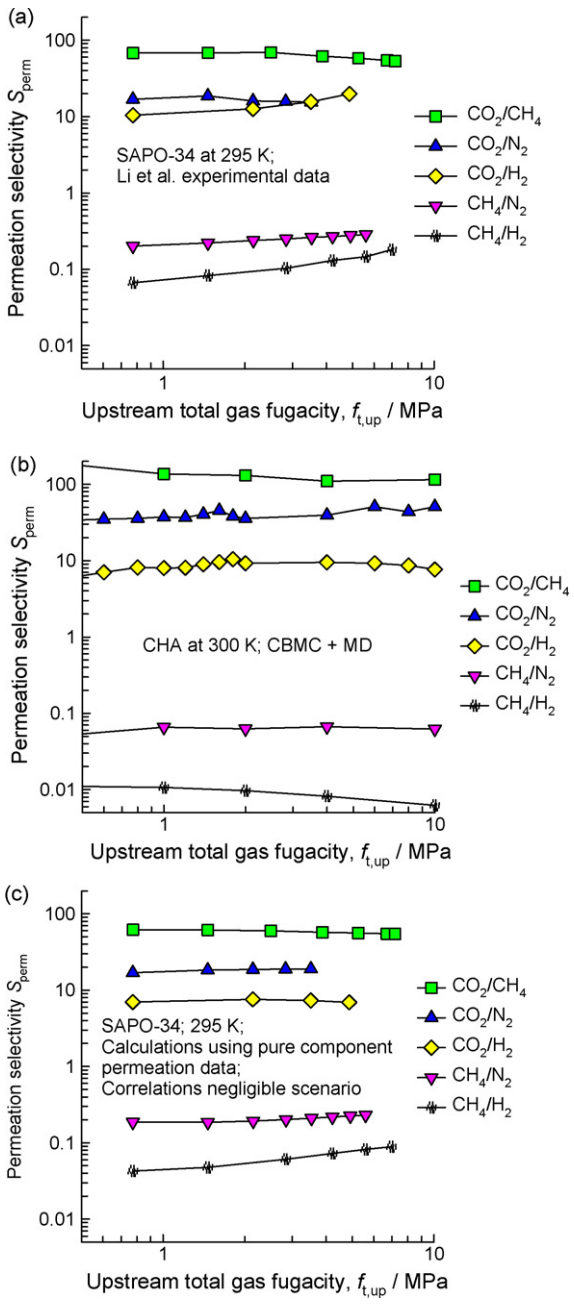


**Fig. 14.** (a) Permeation selectivities, $S_{perm}$, for $CO_2/CH_4$, $CO_2/N_2$, $CO_2/H_2$, $CH_4/N_2$, and $CH_4/H_2$ mixtures obtained from experimental data of Li et al. [49,60] for SAPO-34 membrane at 295 K. (b) Permeation selectivities, $S_{perm}$, from molecular simulations (CBMC, and MD) for CHA at 300 K. (c) Estimations of $S_{perm}$ using the pure component SAPO-34 membrane permeation data, along with the negligible correlations scenario, Eq. (7). Further information on the SAPO-34 modeling is provided in the Supplementary Material.

and $CH_4/H_2$ mixtures across a SAPO-34 membrane at 295 K. SAPO-34 is an iso-type of CHA zeolite, and therefore these data can be compared with molecular simulations of $S_{perm}$ for CHA for the corresponding mixtures; see Fig. 14b. We note that molecular simulations predict the right order of magnitudes for the separation selectivities, along with the correct hierarchy of values for the various mixtures. These results lend confidence in the use of molecular simulations for screening purposes.

For membrane design and development purposes, better estimates of the permeation fluxes and selectivities are obtained by using M–S diffusivities $Đ_i$ that are backed out from unary permeation data, along with experimental pure component isotherms. Using this procedure, described in detail in our earlier work [49,59–61], the calculations of the permeation selectivities for SAPO-34 are presented in Fig. 14c. The agreement of these calculations with the experimental data is better, as is to be expected. In this context, we also draw attention to the recent model of van den Bergh et al. [62].

For more accurate modeling of membrane permeation, there may be a need to also account for inter-crystalline and grain boundary resistances in the polycrystalline membrane layers.

## 4. Conclusions

With the aid of CBMC and MD simulations we have examined the adsorption, diffusion, and permeation selectivities for separation of $CO_2/H_2$, $CO_2/CH_4$, $CO_2/N_2$, $CH_4/N_2$ and $CH_4/H_2$ mixtures using a wide variety of microporous structures, mainly consisting of zeolites. Our investigations provide guidelines to the optimum choice of microporous layers to be used in membrane separations that represent the optimum compromise between $S_{perm}$ and the permeability $\Pi_i$. Specifically, the following major conclusions can be drawn.

(1) For $CO_2$-selective separation of $CO_2/H_2$ mixtures we should aim for microporous structures that have a high degree of correlations, washing out differences in the mobilities of $CO_2$ and $H_2$ molecules. The optimum structure with the best balance between permeation selectivity and permeability is determined to be NaY.
(2) For $CO_2$-selective separation of $CO_2/N_2$ mixtures, NaY zeolite again offers the best balance between $S_{perm}$ and permeability.
(3) For $H_2$-selective separation of $CO_2/H_2$ mixtures, a different strategy needs to be adopted by choosing structures such as ZIF-8 with narrow windows separating cages. The diffusional correlations are negligibly small, and the narrow 0.34 nm result in high $S_{diff}$ values, that overpower the adsorption selectivity in favor of $CO_2$.
(4) For $CO_2$ removal from $CO_2/CH_4$ mixtures the highest $S_{perm}$ are obtained with structures such as ERI, CHA, ITQ-29, and DDR that have narrow 0.35–0.45 nm sized windows separating cages. In such zeolites, the correlation effects are negligibly small. Due to the slenderness of the $CO_2$ molecules, its diffusivities are higher than for partner molecules. For these frameworks, $S_{diff}$ serves to significantly enhance permeation selectivities above the $S_{ads}$ values. The disadvantage of the aforementioned structures is the low permeability, and if the latter is the more desirable property a NaY membrane is a reasonable compromise.
(5) For both $CO_2/N_2$ and $CO_2/CH_4$ separations, the separation performance of a few zeolites exceeds the upper bound of Robeson [44].

We believe that the results presented in this article will help in the development of the appropriate microporous membrane technology for $CO_2$ capture, by appropriate choice of the pore topology with the right degree of diffusional correlations.

## Acknowledgement

RK acknowledges the grant of a TOP subsidy from the Netherlands Foundation for Fundamental Research (NWO-CW) for intensification of reactors.

## Appendix A. Supplementary data

Supplementary data associated with this article can be found, in the online version, at doi:10.1016/j.memsci.2010.05.032.

## Nomenclature

*Nomenclature*

| | |
|---|---|
| $c_i$ | concentration of species $i$ (mol m$^{-3}$) |
| $c_t$ | total concentration in mixture (mol m$^{-3}$) |
| $D_{i,self}$ | self-diffusivity of species $i$ (m$^2$ s$^{-1}$) |
| $Đ_i$ | M–S diffusivity of species $i$ (m$^2$ s$^{-1}$) |
| $Đ_{12}$ | M–S exchange coefficient (m$^2$ s$^{-1}$) |
| $f_i$ | fluid phase fugacity of species $i$ (Pa) |
| $f_t$ | total bulk fluid phase fugacity of mixture (Pa) |
| $\ell$ | thickness of microporous membrane layer (m) |
| $N_i$ | molar flux of species $i$, based on membrane area (mol m$^{-2}$ s$^{-1}$) |
| $p_i$ | partial pressure of species $i$ (Pa) |
| $R$ | gas constant, 8.314 J mol$^{-1}$ K$^{-1}$ |
| $S_{ads}$ | adsorption selectivity |
| $S_{diff}$ | diffusion selectivity |
| $S_{perm}$ | permeation selectivity |
| $T$ | absolute temperature (K) |
| $V_{pore}$ | accessible pore volume (m$^3$ kg$^{-1}$) |
| $x_i$ | mole fraction of species $i$, based on loading within pore |

*Greek letters*

| | |
|---|---|
| $\phi$ | fractional pore volume of microporous material |
| $\mu_i$ | molar chemical potential (J mol$^{-1}$) |
| $\Pi_i$, | permeability of species $i$ across membrane (Barrer) |

*Subscripts*

| | |
|---|---|
| $i$ | referring to component $i$ |
| t | referring to total mixture |

## References

[1] D.M. D'Alessandro, B. Smit, J.R. Long, Carbon dioxide capture: current trends and prospects for new materials, Angew. Chem. Int., 2010, http://dx.doi.org/10.1002/anie.201000431.
[2] M.T. Ho, G.W. Allinson, D.E. Wiley, Reducing the cost of $CO_2$ capture from flue gases using pressure swing adsorption, Ind. Eng. Chem. Res. 47 (2008) 4883–4890.
[3] J. Caro, M. Noack, Zeolite membranes – recent developments and progress, Micropor. Mesopor. Mater. 115 (2008) 215–233.
[4] J. Gascon, F. Kapteijn, Metal–organic framework membranes—high potential, bright future? Angew. Chem. Int. Ed. 49 (2010) 1530–1532.
[5] M. Tagliabue, D. Farrusseng, S. Valencia, S. Aguado, U. Ravon, C. Rizzo, A. Corma, C. Mirodatos, Natural gas treating by selective adsorption: material science and chemical engineering interplay, Chem. Eng. J. 155 (2009) 553–566.
[6] M. Palomino, A. Corma, F. Rey, New insights on $CO_2$–methane separation using LTA zeolites with different Si/Al ratios and a first comparison with MOFs, Langmuir 26 (2010) 1910–1917.
[7] S. Keskin, D.S. Sholl, Screening metal–organic framework materials for membrane-based methane/carbon dioxide separations, J. Phys. Chem. C 111 (2007) 14055–14059.
[8] S. Keskin, D.S. Sholl, Efficient methods for screening of metal organic framework membranes for gas separations using atomically detailed models, Langmuir 25 (2009) 11786–11795.
[9] R. Krishna, J.M. van Baten, Screening of zeolite adsorbents for separation of hexane isomers: a molecular simulation study, Sep. Purif. Technol. 55 (2007) 246–255.

[10] R. Krishna, J.M. van Baten, Using molecular simulations for screening of zeolites for separation of $CO_2/CH_4$ mixtures, Chem. Eng. J. 133 (2007) 121–131.
[11] B. Liu, B. Smit, Comparative molecular simulation study of $CO_2/N_2$ and $CH_4/N_2$ separation in zeolites and metal–organic frameworks, Langmuir 25 (2009) 5918–5926.
[12] T. Düren, Y.S. Bae, R.Q. Snurr, Using molecular simulation to characterise metal–organic frameworks for adsorption applications, Chem. Soc. Rev. 38 (2009) 1237–1247.
[13] R. Babarao, J. Jiang, Diffusion and separation of $CO_2$ and $CH_4$ in silicalite, $C_{168}$ schwarzite, and IRMOF-1: a comparative study from molecular dynamics simulation, Langmuir 24 (2008) 5474–5484.
[14] R. Babarao, J. Jiang, Molecular screening of metal–organic frameworks for $CO_2$ storage, Langmuir 24 (2008) 6270–6278.
[15] Y. Ohta, H. Takaba, S. Nakao, A combinatorial dynamic Monte Carlo approach to finding a suitable zeolite membrane structure for $CO_2/N_2$ separation, Micropor. Mesopor. Mater. 101 (2007) 319–323.
[16] Y.C. Liu, D. Liu, Q. Yang, C. Zhong, J. Mi, Comparative study of separation performance of COFs and MOFs for $CH_4/CO_2/H_2$ mixtures, Ind. Eng. Chem. Res. 49 (2010) 2902–2906.
[17] R. Krishna, Describing the diffusion of guest molecules inside porous structures, J. Phys. Chem. C 113 (2009) 19756–19781.
[18] R. Krishna, J.M. van Baten, Insights into diffusion of gases in zeolites gained from molecular dynamics simulations, Micropor. Mesopor. Mater. 109 (2008) 91–108.
[19] R. Krishna, J.M. van Baten, Onsager coefficients for binary mixture diffusion in nanopores, Chem. Eng. Sci. 63 (2008) 3120–3140.
[20] R. Krishna, J.M. van Baten, Unified Maxwell–Stefan description of binary mixture diffusion in micro- and meso-porous materials, Chem. Eng. Sci. 64 (2009) 3159–3178.
[21] J.M. van de Graaf, F. Kapteijn, J.A. Moulijn, Modeling permeation of binary mixtures through zeolite membranes, AIChE J. 45 (1999) 497–511.
[22] R. Krishna, R. Baur, Modelling issues in zeolite based separation processes, Sep. Purif. Technol. 33 (2003) 213–254.
[23] L. Heinke, D. Tzoulaki, C. Chmelik, F. Hibbe, J.M. van Baten, H. Lim, J. Li, R. Krishna, J. Kärger, Assessing guest diffusivities in porous hosts from transient concentration profiles, Phys. Rev. Lett. 102 (2009) 065901.
[24] D. Tzoulaki, L. Heinke, H. Lim, J. Li, D. Olson, J. Caro, R. Krishna, C. Chmelik, J. Kärger, Assessing surface permeabilities from transient guest profiles in nanoporous host materials, Angew. Chem. Int. Ed. 48 (2009) 3525–3528.
[25] P. Demontis, G.B. Suffritti, A comment on the flexibility of framework in molecular dynamics simulations of zeolites, Micropor. Mesopor. Mater. 125 (2009) 160–168.
[26] K. Seehamart, T. Nanok, J. Kärger, C. Chmelik, R. Krishna, S. Fritzsche, Investigating the reasons for the significant influence of lattice flexibility on self-diffusivity of ethane in Zn(tbip), Micropor. Mesopor. Mater. 130 (2010) 92–96.
[27] K. Seehamart, T. Nanok, R. Krishna, J.M. van Baten, T. Remsungnen, S. Fritzsche, A Molecular Dynamics investigation of the influence of framework flexibility on self-diffusivity of ethane in Zn(tbip) frameworks, Micropor. Mesopor. Mater. 125 (2009) 97–100.
[28] A.F. Combariza, G. Sastre, A. Corma, Propane/propylene diffusion in zeolites: framework dynamics, J. Phys. Chem. C 113 (2009) 11246–11253.
[29] C. Serre, F. Millange, C. Thouvenot, M. Nouguès, G. Marsolier, D. Louër, G. Férey, Very large breathing effect in the first nanoporous chromium(III)-based solids: MIL-53 or $Cr^{III}(OH)\cdot\{O_2C\text{-}C_6H_4\text{-}CO_2\}\cdot\{HO_2C\text{-}C_6H_4\text{-}CO_2H\}_x\cdot H2O_y$, J. Am. Chem. Soc. 124 (2002) 13519–13526.
[30] D. Dubbeldam, R. Krishna, R.Q. Snurr, Method for analyzing the alterations in the crystal structures of metal–organic frameworks, J. Phys. Chem. C 113 (2009) 19317–19327.
[31] R. Krishna, J.M. van Baten, Investigating cluster formation in adsorption of $CO_2$, $CH_4$, and Ar in zeolites and metal organic frameworks at sub-critical temperatures, Langmuir 26 (2010) 3981–3992.
[32] R. Krishna, J.M. van Baten, Comment on comparative molecular simulation study of $CO_2/N_2$ and $CH_4/N_2$ separation in zeolites and metal–organic frameworks, Langmuir 26 (2010) 2975–2978.
[33] R. Krishna, J.M. van Baten, Hydrogen bonding effects in adsorption of water-alcohol mixtures in zeolites and the consequences for the characteristics of the Maxwell–Stefan diffusivities, Langmuir, http://dx.doi.org/10.1021/la100737c.
[34] O. Talu, A.L. Myers, Molecular simulation of adsorption: Gibbs dividing surface and comparison with experiment, AIChE J. 47 (2001) 1160–1168.
[35] A.L. Myers, P.A. Monson, Adsorption in porous materials at high pressure: theory and experiment, Langmuir 18 (2002) 10261–10273.
[36] S. Couck, J.F.M. Denayer, G.V. Baron, T. Rémy, J. Gascon, F. Kapteijn, An amine-functionalized MIL-53 metal–organic framework with large separation power for $CO_2$ and $CH_4$, J. Am. Chem. Soc. 131 (2009) 6326–6327.
[37] J. An, N.L. Rosi, Tuning MOF $CO_2$ adsorption properties via cation exchange, J. Am. Chem. Soc. 132 (2010) 5578–5579.
[38] R. Babarao, J. Jiang, Unprecedentedly high selective adsorption of gas mixtures in RHO zeolite-like metal–organic framework: a molecular simulation study, J. Am. Chem. Soc. 131 (2009) 11417–11425.
[39] D. Dubbeldam, S. Calero, T.J.H. Vlugt, R. Krishna, T.L.M. Maesen, B. Smit, United atom forcefield for alkanes in nanoporous materials, J. Phys. Chem. B 108 (2004) 12301–12313.
[40] K. Makrodimitris, G.K. Papadopoulos, D.N. Theodorou, Prediction of permeation properties of $CO_2$ and $N_2$ through silicalite via molecular simulations, J. Phys. Chem. B 105 (2001) 777–788.
[41] A.I. Skoulidas, D.S. Sholl, Transport diffusivities of $CH_4$, $CF_4$, He, Ne, Ar, Xe, and $SF_6$ in silicalite from atomistic simulations, J. Phys. Chem. B 106 (2002) 5058–5067.
[42] O. Talu, A.L. Myers, Reference potentials for adsorption of helium, argon, methane and krypton in high-silica zeolites, Colloid Surf. A 187–188 (2001) 83–93.
[43] A.V.A. Kumar, H. Jobic, S.K. Bhatia, Quantum effects on adsorption and diffusion of hydrogen and deuterium in microporous materials, J. Phys. Chem. B 110 (2006) 16666–16671.
[44] L.M. Robeson, The upper bound revisited, J. Membr. Sci. 320 (2008) 390–400.
[45] H. Bux, F. Liang, Y. Li, J. Cravillon, M. Wiebcke, J. Caro, Zeolitic imidazolate framework membrane with molecular sieving properties by microwave-assisted solvothermal synthesis, J. Am. Chem. Soc. 131 (2009) 16000–16001.
[46] Y.S. Li, F.Y. Liang, H. Bux, A. Veldhoff, W.S. Yang, J. Caro, Molecular sieve membrane: supported metal–organic framework with high hydrogen selectivity, Angew. Chem. Int. Ed. 49 (2010) 548–551.
[47] Y. Li, F. Liang, H. Bux, W. Yang, J. Caro, Zeolitic imidazolate framework ZIF-7 based molecular sieve membrane for hydrogen separation, J. Membr. Sci. 354 (2010) 48–54.
[48] H.B. Chen, D.S. Sholl, Predictions of selectivity and flux for $CH_4/H_2$ separations using single walled carbon nanotubes as membranes, J. Membr. Sci. 269 (2006) 152–160.
[49] S. Li, J.L. Falconer, R.D. Noble, R. Krishna, Interpreting unary, binary and ternary mixture permeation across a SAPO-34 membrane with loading-dependent Maxwell–Stefan diffusivities, J. Phys. Chem. C 111 (2007) 5075–5082.
[50] M.P. Bernal, J. Coronas, M. Menendez, J. Santamaria, Separation of $CO_2/N_2$ mixtures using MFI-type zeolite membranes, AIChE J. 50 (2004) 127–135.
[51] K. Kusakabe, T. Kuroda, A. Murata, S. Morooka, Formation of a Y-type zeolite membrane on a porous α-alumina tube for gas separation, Ind. Eng. Chem. Res. 36 (1997) 649–655.
[52] Y. Hasegawa, T. Tanaka, K. Watanabe, B.H. Jeong, K. Kusakabe, S. Morooka, Separation of $CO_2$–$CH_4$ and $CO_2$–$N_2$ systems using ion-exchanged FAU-type zeolite membranes with different Si/Al ratios, Korean J. Chem. Eng. 19 (2002) 309–313.
[53] Y. Hasegawa, K. Watanabe, K. Kusakabe, S. Morooka, Influence of alkali cations on permeation properties of Y-type zeolite membranes, J. Membr. Sci. 208 (2002) 415–418.
[54] J.C. White, P.K. Dutta, K. Shqau, H. Verweij, Synthesis of ultrathin zeolite Y membranes and their application for separation of carbon dioxide and nitrogen gases, Langmuir, http://dx.doi.org/10.1021/la100463j.
[55] R. Krishna, J.M. van Baten, Influence of segregated adsorption on mixture diffusion in DDR zeolite, Chem. Phys. Lett. 446 (2007) 344–349.
[56] R. Krishna, J.M. van Baten, Segregation effects in adsorption of $CO_2$ containing mixtures and their consequences for separation selectivities in cage-type zeolites, Sep. Purif. Technol. 61 (2008) 414–423.
[57] S. Himeno, T. Tomita, K. Suzuki, K. Nakayama, S. Yoshida, Synthesis and permeation properties of a DDR-type zeolite membrane for separation of $CO_2/CH_4$ gaseous mixtures, Ind. Eng. Chem. Res. 46 (2007) 6989–6997.
[58] J. van den Bergh, W. Zhu, J. Gascon, J.A. Moulijn, F. Kapteijn, Separation and permeation characteristics of a DD3R zeolite membrane, J. Membr. Sci. 316 (2008) 35–45.
[59] R. Krishna, J.M. van Baten, E. García-Pérez, S. Calero, Incorporating the loading dependence of the Maxwell–Stefan diffusivity in the modeling of $CH_4$ and $CO_2$ permeation across zeolite membranes, Ind. Eng. Chem. Res. 46 (2007) 2974–2986.
[60] R. Krishna, S. Li, J.M. van Baten, J.L. Falconer, R.D. Noble, Investigation of slowing-down and speeding-up effects in binary mixture permeation across SAPO-34 and MFI membranes, Sep. Purif. Technol. 60 (2008) 230–236.
[61] S. Li, J.L. Falconer, R.D. Noble, R. Krishna, Modeling permeation of $CO_2/CH_4$, $CO_2/N_2$, and $N_2/CH_4$ mixtures across SAPO-34 membrane with the Maxwell–Stefan equations, Ind. Eng. Chem. Res. 46 (2007) 3904–3911.
[62] J. van den Bergh, S. Ban, T.J.H. Vlugt, F. Kapteijn, Modeling the loading dependency of diffusion in zeolites: the relevant site model, J. Phys. Chem. C 113 (2009) 17840–17850.